

Ammonia Borane, NH_3BH_3 : A Threshold Photoelectron–Photoion Coincidence Study of a Potential Hydrogen-Storage Material

Domenik Schleier,^[a, b] Marius Gerlach,^[a] Deb Pratim Mukhopadhyay,^[a, c] Emil Karaev,^[a] Dorothee Schaffner,^[a] Patrick Hemberger,^{*, [d]} and Ingo Fischer^{*, [a]}

Abstract: We have investigated the photoionization of ammonia borane (AB) and determined adiabatic ionization energy to be 9.26 ± 0.03 eV for the $X^+ \ ^2E \leftarrow X \ ^1A_1$ transition. Although the threshold photoelectron spectrum appears at first glance to be similar to the one of the isosteric ethane, the electronic situation differs markedly, due to different orbital energies. In addition, an appearance energy AE_{0K^-}

(NH_3BH_3 , NH_3BH_2^+) = 10.00 ± 0.03 eV has been determined, corresponding to the loss of a hydrogen atom at the BH_3 -site. From the data, a 0 K bond dissociation energy for the B–H bond in the cation of 71.5 ± 3 kJ mol⁻¹ was derived, whereas the one in the neutral compound has been estimated to be 419 ± 10 kJ mol⁻¹.

Introduction

Improving hydrogen-storage capabilities is one of the prime challenges to establishing an environmentally friendly, circular economy. Various methods have been developed that range from liquification, via adsorption onto metals or (metal) organic-frameworks,^[1] to chemical conversion that stores hydrogen by incorporating it into a different compound. Although the accessibility of H_2 is better with liquification or adsorption techniques,^[2] the highest (volumetric) density is achieved by chemically converting it into hydrogen carrier molecules like ammonia,^[3] methanol,^[4] or ammonia borane (AB).^[5] In particular,

AB has attracted attention, and its potential in different applications has been described in several reviews.^[6]

It has been intensively investigated in the solid state,^[7] yet gas-phase studies required to obtain accurate structural and thermochemical information are scarce. Nearly all authors reported weak signals due to the extremely low vapor pressure and rapid decomposition while trying to heat the samples.^[8] The first gas phase study of AB was performed in 1970 by Lloyd and Lynaugh, who investigated its photoionization using photoelectron spectroscopy.^[8a] They found a vertical ionization energy (IE) of 10.33 ± 0.04 eV, but noted that their spectrum is of low quality as a result of partial degradation. Later they expanded their initial findings by measuring the adiabatic IE at 9.44 ± 0.02 eV.^[9] More than ten years later, two microwave studies determined the B–N bond length, dipole moment, rotational barrier and zero-point structures in AB.^[10] The work was later expanded by observing the quadrupole splitting.^[11] First studies on the vibrational spectroscopy of AB were conducted by matrix isolation, and determined the N–¹¹B stretch mode to be 968 cm⁻¹.^[7e] The first gas-phase IR spectrum was reported by Sams et al. in 2012, who achieved rotational resolution (> 0.0035 cm⁻¹) using a 68 m effective path length IR cell.^[8b] They corrected the assignment of the N–¹¹B stretch mode to 603 cm⁻¹, which was recently corroborated by anharmonic vibrational computations.^[12] This proved that the N–B stretch reacts sensitively to the environment that AB is embedded in, and underlined the need for gas-phase studies on isolated AB.


Ionization and appearance energies (AEs) can be used to determine bond enthalpies, which are a prerequisite to establish the thermochemistry of individual steps in the H_2 release and recovery cycle. Yet, for AB these data are only available from computational studies.^[13] Here, we employed synchrotron radiation to investigate the photoionization of AB to determine its adiabatic IE and the appearance energy (AE) of


[a] Dr. D. Schleier, M. Gerlach, Dr. D. Pratim Mukhopadhyay, E. Karaev, D. Schaffner, Prof. I. Fischer
Institute of Physical and Theoretical Chemistry
University of Würzburg
Am Hubland, 97074 Würzburg (Germany)
E-mail: ingo.fischer@uni-wuerzburg.de

[b] Dr. D. Schleier
Present Address: Laboratory for Astrophysics
Leiden Observatory, Leiden University
2300 RA Leiden (The Netherlands)

[c] Dr. D. Pratim Mukhopadhyay
Present address: Department of Dynamics of Molecules and Clusters
J. Heyrovský Institute of Physical Chemistry
Dolejškova 2155/3, 182 23 Praha 8 (Czech Republic)

[d] Dr. P. Hemberger
Laboratory for Synchrotron Radiation and Femtochemistry
Paul Scherrer Institut (PSI), 5232 Villigen (Switzerland)
E-mail: patrick.hemberger@psi.ch

 Supporting information for this article is available on the WWW under <https://doi.org/10.1002/chem.202201378>

 © 2022 The Authors. Chemistry - A European Journal published by Wiley-VCH GmbH. This is an open access article under the terms of the Creative Commons Attribution Non-Commercial License, which permits use, distribution and reproduction in any medium, provided the original work is properly cited and is not used for commercial purposes.

its fragments upon dissociative ionization. To avoid potential interference with decomposition products, we employed photoelectron-photoion coincidence (PEPICO) spectroscopy.^[14] In this scheme, electrons and ions from a single ionization event are correlated, leading to photoion mass-selected threshold photoelectron spectra (ms-TPES).^[15] In the past, we applied this approach to record ms-TPE spectra of a number of boron containing molecules,^[16] and revised the bond enthalpy of the B–C bond.^[17] As ms-TPES has the potential to isomer-selectively detect intermediates in reactive flows, combustion, catalysis, atmospheric and astrochemistry, there is a strong need to obtain reference spectra.^[15a,18]

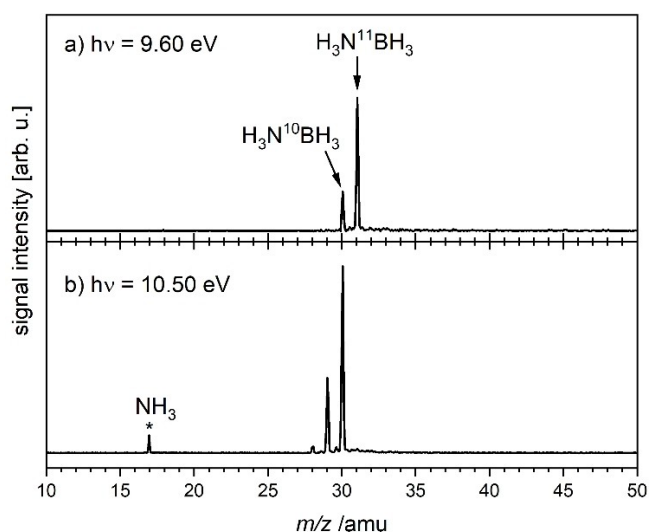


Figure 1. Threshold mass spectra of ammonia borane (NH_3BH_3) at different photon energies. NH_3 is assigned as a decomposition product of ammonia borane.

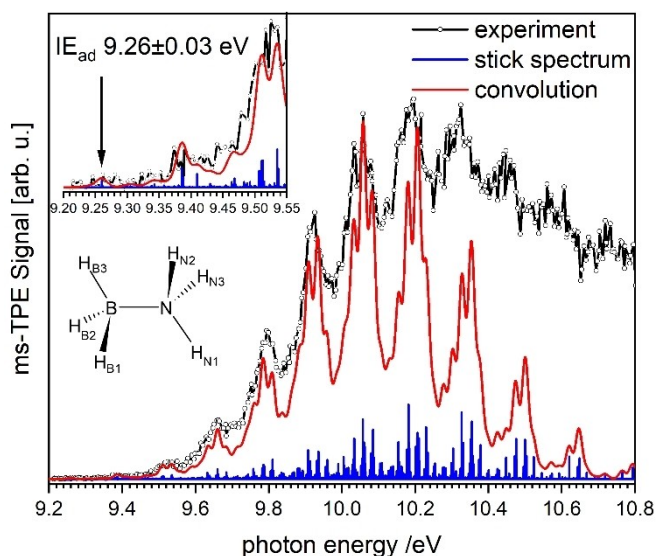


Figure 2. ms-TPES of NH_3BH_3 between 9.20 and 10.80 eV. The IE was determined to be 9.26 ± 0.03 eV (see inset).

Results and Discussion

The threshold mass spectrum of ammonia borane at 9.60 eV is displayed in Figure 1a. At 9.60 eV, the dominant peak is at m/z 31 with a smaller peak being visible at m/z 30. These two can be assigned to the ^{11}B and ^{10}B isotopes of AB, respectively. In the bottom trace the synchrotron light was set to 10.50 eV. A new peak without isotopic pattern at m/z 17 becomes visible, originating from ammonia (IE: 10.07 eV) most likely a decomposition product of AB that has been observed by others as well.^[8b] Due to the mass-selection in the PEPICO scheme, small impurities do not interfere with the ms-TPES of AB. The most intense peak in Figure 1b is at m/z 30, indicating a hydrogen atom loss from AB by dissociative photoionization (DPI) between 9.60 and 10.50 eV. The presence of mass 28 at 10.50 eV, may be associated with the onset of a second hydrogen loss in AB at higher photon energies.

The ms-TPE spectrum of AB is shown in Figure 2 together with a Franck–Condon (FC) simulation. To account for the dissociative photoionization that sets in between 9.60 and 10.50 eV, all mass channels from 28 to 31 have been included in the analysis. The first small peak can be seen at 9.37 eV, and a second more clear band comes up around 9.50 eV. Up to this energy the spectrum does not exhibit any clear vibrational structure. Starting at 9.66 eV, bands appear at regular intervals of 1150 cm^{-1} up to 10.35 eV. However, above 10.00 eV the bands give rise to (multiple) separated satellites, thus indicating that these bands contain more than one dominant vibrational transition. Above 10.4 eV the signal intensity starts to decline, until a FC-gap region is reached between 11.5 and 12 eV, where the overall signal intensity is low. Increasing the photon energy further also increases the TPE signal, which may originate from an excited state in the cation, depicted in Figure S1 in the Supporting Information.

Similar to Lloyd and Lynaugh,^[9] it is tempting to attribute the vibrational progression in the cation to a single mode and determine the onset of the spectrum at 9.37 eV as the IE_{adr} , yet ionization processes can be complex as seen in other boron containing compounds.^[16b]

In order to get more detailed insight into the spectrum, quantum chemical calculations of the neutral and cation have been performed, using density functional theory (DFT) with the ωB97XD functional and a 6–311+Laboratory for Synchrotron Radiation and Femtochemistry + G(d,p) basis set.

AB in its neutral ground state exhibits a C_{3v} symmetry with staggered hydrogen atoms in line with previous high level computations.^[8b,12] A low rotational barrier of 8.66 kJ mol^{-1} around the B–N bond has been found.^[10b] The bond lengths and angles of the neutral and cation can be found in Table 1, where hydrogens on the boron are marked as $\text{H}_{\text{B}1-3}$ and hydrogens on the nitrogen are $\text{H}_{\text{N}1-3}$, respectively.

Upon ionization, the B–N bond length decreases by more than 0.1 \AA . At the NH_3 subunit almost no change is observed, but the bond lengths and angles on the BH_3 site show major displacements. Interestingly, two B–H bond distances increase while the third decreases. Thus, the symmetry is reduced to C_s .

Table 1. Structural parameters for ammonia borane. Experimental values were taken from ref. [10b]. Neutral and cation values were calculated by DFT (ω B97XD/6-311 + + G(d,p)).

Parameter	Neutral	Experiment	Cation
$d(\text{B-N})/\text{\AA}$	1.663	1.672	1.555
$d(\text{B-H}_{\text{B}_1})/\text{\AA}$	1.208	1.210	1.271
$d(\text{B-H}_{\text{B}_2})/\text{\AA}$	1.208	1.210	1.271
$d(\text{B-H}_{\text{B}_3})/\text{\AA}$	1.208	1.210	1.173
$d(\text{N-H}_{\text{N}_1})/\text{\AA}$	1.017	1.014	1.024
$d(\text{N-H}_{\text{N}_2})/\text{\AA}$	1.017	1.014	1.027
$d(\text{N-H}_{\text{N}_3})/\text{\AA}$	1.017	1.014	1.027
$(\text{H}_{\text{B}_1}\text{BH}_{\text{B}_2})/^\circ$	113.7	113.9	55.9
$(\text{H}_{\text{B}_2}\text{BH}_{\text{B}_3})/^\circ$	113.7	113.9	119.9
$(\text{H}_{\text{B}_3}\text{BH}_{\text{B}_1})/^\circ$	113.7	113.9	119.9
$(\text{H}_{\text{N}_1}\text{NH}_{\text{N}_2})/^\circ$	107.8	109.1	107.2
$(\text{H}_{\text{N}_2}\text{NH}_{\text{N}_3})/^\circ$	107.8	109.1	105.7
$(\text{H}_{\text{N}_3}\text{NH}_{\text{N}_1})/^\circ$	107.8	109.1	107.2

Consequently, the ejected electron must originate from an antibonding BN orbital with some contributions towards the BH bonds. Indeed, our calculations predict two degenerate HOMOs for AB with π_x and π_y character, which have antibonding character with respect to the B–N bond, but are bonding towards the respective hydrogen atoms. One of these orbitals exhibits a nodal plane that intersects the H_{B_3} –B–N– H_{N_1} plane, rendering the two corresponding B–H and N–H bonds less affected by the ionization. The decrease in the B–H bond length presumably originates from electrostatic effects. Due to the difference in electronegativity of B and N, the electron hole resides mostly on the BH_3 site, shifting the electron density in the B– H_{B_3} bond towards the boron. The three highest occupied MOs are displayed in Figure 3.

Removal of an electron from the neutral species does not guarantee that the fundamental transition, that is, the adiabatic IE, is visible in the ensuing TPE spectrum, especially if the geometry changes significantly upon ionization. Furthermore, the transitions may be affected by the coupling strength between different electronic states, that is, (pseudo)Jahn–Teller

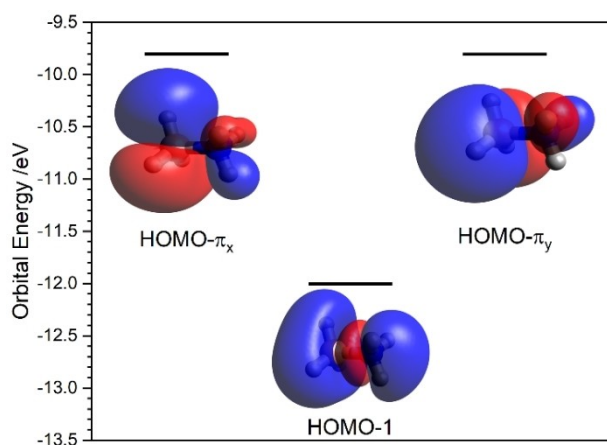


Figure 3. The three highest occupied molecular orbitals in neutral AB. Note that $\text{HOMO-}\pi_x$ and $\text{HOMO-}\pi_y$ are degenerate. The NH_3 unit is on the right; the BH_3 unit is on the left.

distortions. From our calculations we can estimate that the geometric distortion in AB is significant, in line with the vibrational progression in the experimental spectrum. Yet, DFT methods are generally unsuited to quantify electronic or vibronic couplings. The lack of high-level computational data in the literature has prompted us to estimate these effects based on comparisons to its hydrocarbon congener ethane.

Although ethane is one of the simplest hydrocarbons, its cationic potential energy surface has only recently been fully characterized by experiments and theory.^[19] Near the ionization threshold, the ejected electron can originate from three orbitals, the two degenerate C–H binding HOMOs of e_g symmetry or the C–C binding a_{1g} orbital around 0.36 eV (EOMIP-CCSD/ANO)^[19b] or 0.73 eV (ω B97XD/6-311 + + G(d,p)) below the first two. The 2E_g symmetry enforces a Jahn–Teller splitting of the ionic ground state. Furthermore, due to their quasi isoenergeticity, in ethane the excited $A^+{}^2A_{1g}$ state couples efficiently to the $X^+{}^2E_g$ ground state, which results in an additional pseudo-Jahn–Teller (PJT) distortion in the cation. The latter leads to two different equilibrium geometries, a “diborane-like” (DB) C_{2h} and a “long-bond” (LB) D_{3d} structure for the 2E_g and ${}^2A_{1g}$ state, respectively. The energy difference between the two states has been calculated to be only 250 cm^{-1} (3 kJ mol^{-1}).^[20]

Comparison of the photoelectron spectra of ethane and AB allows us to rationalize whether similar effects are present in AB as well. The photoelectron spectrum of ethane exhibits an equidistant band structure with spacings of 1170 cm^{-1} , which was initially attributed to the vibrational progression of the symmetric C–H deformation mode.^[21] Yet, the progression can only be adequately described using quadratic coupling terms for the PJT and JT active modes, due to the LB and DB structures being almost isoenergetic.^[19b] Therefore, the bands originate from intense vibronic couplings between the 2E_g and ${}^2A_{1g}$ states.

An almost identical vibrational structure can be seen in Figure 2, with spacings of 1150 cm^{-1} ; this indicates a high similarity between the two molecules. However, despite the potentially complex situation, our FC simulation for AB matches the experimental spectrum very well when the IE_{ad} is set to $9.26 \pm 0.03\text{ eV}$. For example, the splitting of the band around 10.06 eV in three components is well represented in the simulation. Shifting the FC simulation within ± 1 vibrational band on the photon energy axis, leads to an inferior fit. In addition, the experimental value is in excellent agreement with the calculated IE_{ad} of 9.29 (G4), 9.31 (CBS-QB3), 9.28 (CBS-APNO), 9.25 (W1) and 9.30 eV (G3) as well as computational values in the literature (9.29 eV) and is thus assigned to our experimental IE_{ad} .^[13]

Discussing the goodness of our FC simulation is also warranted. The simulation in Figure 2 includes up to four quanta in the cationic vibrations, which coincides well with the experimental trace. At lower energies the FC simulation shows a better resolved structure and the individual bands are better separated. This can be mostly attributed to differences in the real rotational envelope of the experiment and the assumed one in the simulation. At higher energies ($> 10.4\text{ eV}$) the experimental spectrum has higher intensities than the FC

simulation, which can be largely attributed to the presence of transitions requiring more than four quanta in the cation in this energy region. The less pronounced separation of the individual bands in this energy region can be attributed to an increased anharmonicity. Contributions from other electronic states can be excluded based on our calculations, which show no indication for the presence of other states up to 12 eV (Figure S1). Since the BNH_6 potential energy surface has only one stable isomer, no other isomeric contributions are expected. Including more than four quanta in the FC simulation results in a steadily increasing photoelectron signal at higher photon energies, which deviates fully from the experimental spectrum (Figure S2). One possible explanation could be the low torsional motion barrier (275 cm^{-1} in the neutral and 180 cm^{-1} in the cation) along the B–N bond, which is strongly anharmonic and cannot be treated using the harmonic Franck–Condon factor calculations used in this study. Nevertheless, considering the computational effort that is needed to simulate the photoelectron spectrum of ethane, it is surprising that our FC simulation for AB agrees well with the experimental spectrum in the low photon energy range and the 0–0 transition matches very well with the calculated adiabatic IEs.

Hence, we conclude, that the electronic structures in the cations of ethane and AB differ significantly from each other. The HOMO-1, that represents the σ -bonding orbital between boron and nitrogen in AB, is roughly 2.2 eV ($\omega\text{B97XD/6-311}++\text{G(d,p)}$) below the two degenerate HOMOs. Hence, the PJT effect is significantly less pronounced, shifting the corresponding ${}^2\text{A}_1$ state and its LB structure upwards in energy.

This might leave the AB cation only subject to a JT distortion. If the barrier between the minima is high and the ion is trapped in one minimum energy configuration, the calculation of the cationic ground state even on a relatively low computational level lead to an adequate FC simulation. Yet, while the experimental spectrum initially suggests an equidistant spacing in the vibrational progression, and thus activity in a single vibration, the FC simulation predicts multiple equally intense transitions within one band. Although they coincide with a H–B–H bending (1136 cm^{-1}) vibration in the cation, the individual transitions of the simulation show contributions from up to four different vibrational modes and can thus not be directly assigned. To resolve these bands further, higher-resolution zero kinetic energy (ZEKE) photoelectron spectroscopy may be required.^[22]

Ms-TPE spectroscopy allows the appearance energy (AE) for hydrogen loss in AB^+ to be determined. As different kinds of hydrogen exist in the molecule, it is important to determine which hydrogen is the most weakly bound in the cation. Whereas there are two sets of hydrogens in the neutral, hydridic ($\text{H}_{\text{B}1-3}$) and protic ($\text{H}_{\text{N}1-3}$), the cation exhibits four different hydrogens, two on each side. In general, N–H bond energies are found to be stronger as compared to B–H in the cation according to the literature.^[23] The appearance energy of the first hydrogen loss at the boron site is calculated to be 10 eV, which is in excellent agreement with the breakdown diagram (Figure 4), showing an onset at around 10 eV.^[23]

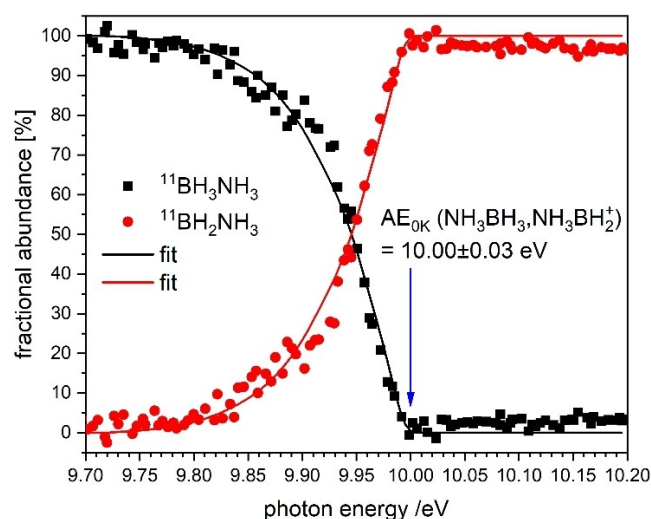


Figure 4. Breakdown diagram of the hydrogen loss for AB^+ . The hydrogen is lost on the boron atom, and an $\text{AE}_{0\text{K}}$ of $10.00 \pm 0.03\text{ eV}$ was determined.

The corresponding breakdown diagram (BD) is depicted from 9.70 to 10.20 eV in Figure 4. It was recorded with steps of 5 meV and each point was averaged for 30 s. It has been corrected for the two boron isotopes by eliminating all contributions from any ${}^{10}\text{B}$ species, using statistical abundances. Mass spectra at the dissociation threshold were symmetric, hence no kinetic shift of the AE is expected, and the breakdown diagram only corresponds to the integral of the energy distribution in the cation. This energy distribution is created by calculating the energy distribution of the neutral species and consequently shifting it into the ion manifold. The model relies on the harmonic Boltzmann distribution to calculate the internal energy of the neutral, which is implemented in the miniPEPICO suite of programs.^[24] For the simulation a vibrational temperature of 305 K was assumed, in agreement with the sample temperature. The $\text{AE}_{0\text{K}}$ is fitted to the point, where the parent signal (${}^{11}\text{BH}_3\text{NH}_3$) converges to zero, that is, the energy at which molecules in the rovibronic ground state are excited to the threshold of dissociative photoionization. It has been determined to be $10.00 \pm 0.03\text{ eV}$. As no reverse barrier was computed for the hydrogen loss reaction, the dissociation energy for the hydrogen loss at the boron site (corresponding to the bond dissociation energy, BDE at 0 K) of $(\text{NH}_3\text{BH}_3)^+$ is calculated from $\text{AE}_{0\text{K}} - \text{IE}_{\text{ad}}$ to be $\text{D}_0^+ = 0.74 \pm 0.03\text{ eV}$ ($71.5 \pm 3\text{ kJ mol}^{-1}$).

Note that the cation exhibits deeper wells along other internal coordinates. Therefore, we see B–H dissociation taking place at 10.00 eV, but the vibrational structure in the TPES (Figure 2) continues, since it involves different coordinates.

The AE can further be used in a thermochemical cycle to determine the BDE of the B–H bond in neutral AB by using Equation (1).

$$\text{BDE}(\text{H}_3\text{NH}_2\text{B}-\text{H}) = \text{AE}_{0\text{K}}(\text{NH}_3\text{BH}_3, \text{NH}_3\text{BH}_2^+) - \text{IE}(\text{NH}_3\text{BH}_2) \quad (1)$$

Unfortunately, the IE of NH_3BH_2 is not known experimentally. With the computed value of $5.65\text{ eV}^{[13]}$ the BDE can be determined to be $419 \pm 10\text{ kJ mol}^{-1}$. The error bars assume that computed IE_{ad} are generally accurate to within 0.1 eV . This BDE is in very good agreement with the value of 422 kJ mol^{-1} calculated on the CBS-QB3 level of theory. Obviously, the B–H bond is much stronger in the neutral as compared to the cation, which may be explained by a significant destabilization of this bond in the cation due to electronic effects.

Conclusion

The photoionization of ammonia borane (AB) has been investigated using imaging photoelectron photoion coincidence spectroscopy. The molecule attracts widespread interest as a potential hydrogen storage compound.^[6] AB was heated to 45°C and introduced directly into the experimental chamber. Based on a Franck–Condon simulation, an adiabatic ionization energy of $9.26 \pm 0.03\text{ eV}$ was determined. Comparison of AB and its hydrocarbon analogue ethane offers insights into the electronic situation of the AB cation. After ionization, the situation in ethane is rather complex, due to the combination of a Jahn–Teller and a pseudo-Jahn–Teller effect, thus requiring tremendous effort to characterize the potential energy surface.^[19] For AB, on the other hand, good agreement between experiment and simulations was achieved at the DFT level. This is attributed to the larger energy gap between the relevant molecular orbitals of AB. Furthermore, the electronegativity differences between N and B increases the contributions of the boron atom to the degenerate HOMOs.

The dissociative photoionization of AB reveals a hydrogen loss at the boron site. Modeling using statistical unimolecular rate theory determines no kinetic shift. A barrier of 0.74 eV and an $\text{AE}_{0\text{K}}$ of $10.00 \pm 0.03\text{ eV}$ were found. By using these values together with the IE of NH_3BH_2 , the dissociation energy for the B–H bond in AB can be determined as $419 \pm 10\text{ kJ mol}^{-1}$. These improved thermochemical values might lead to a better understanding of the elementary reaction steps involved in the storage and release of H_2 .

Experimental Section

Experiments were performed at the X04DB Vacuum Ultraviolet beamline at the Swiss Light Source (SLS). The double imaging CRF-PEPICO (combustion reactions followed by PEPICO) spectrometer was employed.^[25] Ammonia borane (ABCR, 97%) was placed in an effusive sample container (SC) and heated to 45°C . The SC was directly connected to the experimental chamber where the pressure was around $2.0 \times 10^{-7}\text{ mbar}$. Under these conditions, the vapor pressure of AB was high enough for gas-phase measurements. The neutral molecules inside the chamber were ionized using synchrotron radiation (SR), provided by a bending magnet. The SR was collimated and diffracted using a plane grating (150 lines/mm) with a resolution of $E/\Delta E = 1500$. Higher harmonics were suppressed by a noble gas filter, limiting the range of the photon energy between 7 and 14 eV during the experiments. The photon energy was calibrated using the $11\text{ s}'\text{--}14\text{ s}'$ autoionization resonan-

ces of Ar in the first and second order of the grating. A detailed description of the beamline is given elsewhere.^[25a] Electrons and ions were detected in coincidence using a multiple-start/multiple-stop scheme and both particles were imaged on two position sensitive Roentdeck DLD40 delay line detectors. Threshold electrons were collected with a resolution of 5 meV and contributions of hot electrons were subtracted following the procedure by Sztaray and Baer.^[26] The TPE signals have been normalized to the photon flux and shifted by $+88\text{ cm}^{-1}$ to account for the extraction field.

Geometry optimizations followed by calculations of harmonic frequencies in both neutral and cationic states were performed using the CBS-QB3, G3, G4, CBS-APNO and W1 composite approaches and density functional theory (DFT) using the $\omega\text{B97XD}/6\text{-311++G(d,p)}$ method, both contained in the Gaussian 09 program package.^[27] Adiabatic ionization energies were calculated from the difference between the zero-point energies of neutral and cationic species. Threshold photoelectron spectra were simulated using the program ezSpectrum.^[28] FC simulations have been performed at room temperature and within the harmonic approximation. All vibrations of the cation and the neutral were included, but excitations in the cation were limited to four quanta for the simulation. The FC-factors were calculated and the stick spectrum convoluted with a Gaussian function of 20 meV full-width half maximum (FWHM).

Acknowledgements

The experiments were performed at the VUV beamline of the Swiss Light Source, located at the Paul Scherrer Institute (PSI). The work was financially supported by the Deutsche Forschungsgemeinschaft (DFG), contract FI575/13-2 and GRK 2112. D.S. acknowledges support by the PRIME programme of the German Academic Exchange Service (DAAD) with funds from the German Federal Ministry of Education and Research (BMBF). Open Access funding enabled and organized by Projekt DEAL.

Conflict of Interest

There are no conflicts to declare.

Data Availability Statement

The data that support the findings of this study are available from the corresponding author upon reasonable request.

Keywords: ammonia borane · hydrogen storage · Jahn–Teller effect · molecular orbitals · photoelectron spectroscopy

- [1] V. Stavila, S. Li, C. Dun, M. A. T. Marple, H. E. Mason, J. L. Snider, J. E. Reynolds III, F. El Gabaly, J. D. Sugar, C. D. Spataru, X. Zhou, B. Dizdar, E. H. Majzoub, R. Chatterjee, J. Yano, H. Schlomberg, B. V. Lotsch, J. J. Urban, B. C. Wood, M. D. Allendorf, *Angew. Chem. Int. Ed.* **2021**, *60*, 25815–25824.
- [2] P. Jena, *J. Phys. Chem. Lett.* **2011**, *2*, 206–211.
- [3] H. Kobayashi, A. Hayakawa, K. D. Kunkuma, A. Somarathne, E. C. Okafor, *Proc. Combust. Inst.* **2019**, *37*, 109–133.
- [4] A. Kumar, P. Daw, D. Milstein, *Chem. Rev.* **2022**, *122*, 385–441.

- [5] a) U. B. Demirci, *Energies* **2020**, *13*, 3071; b) G. Zhang, D. Morrison, G. Bao, H. Yu, C. W. Yoon, T. Song, J. Lee, A. T. Ung, Z. Huang, *Angew. Chem. Int. Ed.* **2021**, *60*, 11725–11729.
- [6] a) F. H. Stephens, V. Pons, R. Tom Baker, *Dalton Trans.* **2007**, 2613–2626; b) T. B. Marder, *Angew. Chem. Int. Ed.* **2007**, *46*, 8116–8118; *Angew. Chem.* **2007**, *119*, 8262–8264; c) C. D. Mboyi, D. Poinso, J. Roger, K. Fajerweg, M. L. Kahn, J.-C. Hierso, *Small* **2021**, *17*, 2102759; d) U. Eberle, M. Felderhoff, F. Schüth, *Angew. Chem. Int. Ed.* **2009**, *48*, 6608–6630; *Angew. Chem.* **2009**, *121*, 6732–6757.
- [7] a) R. C. Taylor, C. L. Cluff, *Nature* **1958**, *182*, 390–391; b) S. Trudel, D. F. R. Gilson, *Inorg. Chem.* **2003**, *42*, 2814–2816; c) R. Custelcean, Z. A. Dreger, *J. Phys. Chem. B* **2003**, *107*, 9231–9235; d) N. J. Hess, M. E. Bowden, V. M. Parvanov, C. Mundy, S. M. Kathmann, G. K. Schenter, T. Autrey, *J. Chem. Phys.* **2008**, *128*, 034508; e) J. Smith, K. S. Seshadri, D. White, *J. Mol. Spectrosc.* **1973**, *45*, 327–337; f) E. C. Reynhardt, C. F. Hoon, *J. Phys. C* **1983**, *16*, 6137–6152; g) G. H. Penner, Y. C. P. Chang, J. Hutzal, *Inorg. Chem.* **1999**, *38*, 2868–2873; h) O. Gunaydin-Sen, R. Achey, N. S. Dalal, A. Stowe, T. Autrey, *J. Phys. Chem. B* **2007**, *111*, 677–681; i) D. G. Allis, M. E. Kosmowski, B. S. Hudson, *J. Am. Chem. Soc.* **2004**, *126*, 7756–7757; j) C. F. Hoon, E. C. Reynhardt, *J. Phys. C* **1983**, *16*, 6129–6136; k) W. T. Klooster, T. F. Koetzle, P. E. M. Siegbahn, T. B. Richardson, R. H. Crabtree, *J. Am. Chem. Soc.* **1999**, *121*, 6337–6343.
- [8] a) D. R. Lloyd, N. Lynaugh, *J. Chem. Soc. D* **1970**, 1545–1546; b) R. L. Sams, S. S. Xantheas, T. A. Blake, *J. Phys. Chem. A* **2012**, *116*, 3124–3136.
- [9] D. R. Lloyd, N. Lynaugh, *J. Chem. Soc. Faraday Trans. 2* **1972**, *68*, 947–958.
- [10] a) R. D. Suenram, L. R. Thorne, *Chem. Phys. Lett.* **1981**, *78*, 157–160; b) L. R. Thorne, R. D. Suenram, F. J. Lovas, *J. Chem. Phys.* **1983**, *78*, 167–171.
- [11] K. Vormann, H. Dreizler, *Z. Naturforsch. A* **1991**, *46*, 1060–1062.
- [12] B. R. Westbrook, E. M. Valencia, S. C. Rushing, G. S. Tschumper, R. C. Fortenberry, *J. Chem. Phys.* **2021**, *154*, 041104.
- [13] M. H. Matus, D. J. Grant, M. T. Nguyen, D. A. Dixon, *J. Phys. Chem. C* **2009**, *113*, 16553–16560.
- [14] T. Baer, R. P. Tuckett, *Phys. Chem. Chem. Phys.* **2017**, *19*, 9698–9723.
- [15] a) I. Fischer, S. T. Pratt, *Phys. Chem. Chem. Phys.* **2022**, *24*, 1944–1959; b) J. M. Dyke, *Phys. Chem. Chem. Phys.* **2019**, *21*, 9106–9136.
- [16] a) D. Schleier, A. Humeniuk, E. Reusch, F. Holzmeier, D. Nunez-Reyes, C. Alcaraz, G. A. Garcia, J.-C. Loison, I. Fischer, R. Mitric, *J. Phys. Chem. Lett.* **2018**, *9*, 5921–5925; b) D. P. Mukhopadhyay, D. Schleier, I. Fischer, J. C. Loison, C. Alcaraz, G. A. Garcia, *Phys. Chem. Chem. Phys.* **2020**, *22*, 1027–1034; c) D. Schleier, D. Schaffner, M. Gerlach, P. Hemberger, I. Fischer, *Phys. Chem. Chem. Phys.* **2022**, *24*, 20–24; d) K. H. Fischer, M. Schneider, I. Fischer, B. Pfaffinger, H. Braunschweig, B. Sztáray, A. Bodi, *Chem. Eur. J.* **2012**, *18*, 4533–4540; e) F. Holzmeier, M. Lang, P. Hemberger, A. Bodi, M. Schäfer, R. D. Dewhurst, H. Braunschweig, I. Fischer, *Chem. Eur. J.* **2014**, *20*, 9683–9692.
- [17] D. P. Mukhopadhyay, D. Schleier, S. Wirsing, J. Ramler, D. Kaiser, E. Reusch, P. Hemberger, T. Preitschopf, I. Krummenacher, B. Engels, I. Fischer, C. Lichtenberg, *Chem. Sci.* **2020**, *11*, 7562–7568.
- [18] P. Hemberger, A. Bodi, T. Bierkandt, M. Köhler, D. Kaczmarek, T. Kasper, *Energy Fuels* **2021**, *35*, 16265–16302.
- [19] a) U. Jacovella, C. J. Stein, M. Grütter, L. Freitag, C. Lauzin, M. Reiher, F. Merkt, *Phys. Chem. Chem. Phys.* **2018**, *20*, 1072–1081; b) K. L. K. Lee, S. M. Rabidoux, J. F. Stanton, *J. Phys. Chem. A* **2016**, *120*, 7548–7553.
- [20] H. M. Sulzbach, D. Graham, J. C. Stephens, H. F. Schaefer III, *Acta Chem. Scand.* **1997**, *51*, 547–555.
- [21] A. D. Baker, C. Baker, C. R. Brundle, D. W. Turner, *Int. J. Mass Spectrom. Ion Phys.* **1968**, *1*, 285–301.
- [22] K. Müller-Dethlefs, E. W. Schlag, *Angew. Chem. Int. Ed.* **1998**, *37*, 1346–1374; *Angew. Chem.* **1998**, *110*, 1414–1444.
- [23] B. Yuan, J.-W. Shin, E. R. Bernstein, *J. Chem. Phys.* **2016**, *144*, 144315.
- [24] B. Sztáray, A. Bodi, T. Baer, *J. Mass Spectrom.* **2010**, *45*, 1233–1245.
- [25] a) M. Johnson, A. Bodi, L. Schulz, T. Gerber, *Nucl. Instrum. Methods Phys. Res. Sect. A* **2009**, *610*, 597–603; b) B. Sztáray, K. Voronova, K. G. Torma, K. J. Covert, A. Bodi, P. Hemberger, T. Gerber, D. L. Osborn, *J. Chem. Phys.* **2017**, *147*, 013944.
- [26] B. Sztáray, T. Baer, *Rev. Sci. Instrum.* **2003**, *74*, 3763–3768.
- [27] M. J. Frisch, G. W. Trucks, H. B. Schlegel, G. E. Scuseria, M. A. Robb, J. R. Cheeseman, G. Scalmani, V. Barone, G. A. Petersson, H. Nakatsuji, X. Li, M. Caricato, A. V. Marenich, J. Bloino, B. G. Janesko, R. Gomperts, B. Mennucci, H. P. Hratchian, J. V. Ortiz, A. F. Izmaylov, J. L. Sonnenberg, Williams, F. Ding, F. Lipparini, F. Egidi, J. Goings, B. Peng, A. Petrone, T. Henderson, D. Ranasinghe, V. G. Zakrzewski, J. Gao, N. Rega, G. Zheng, W. Liang, M. Hada, M. Ehara, K. Toyota, R. Fukuda, J. Hasegawa, M. Ishida, T. Nakajima, Y. Honda, O. Kitao, H. Nakai, T. Vreven, K. Throssell, J. A. Montgomery Jr., J. E. Peralta, F. Ogliaro, M. J. Bearpark, J. J. Heyd, E. N. Brothers, K. N. Kudin, V. N. Staroverov, T. A. Keith, R. Kobayashi, J. Normand, K. Raghavachari, A. P. Rendell, J. C. Burant, S. S. Iyengar, J. Tomasi, M. Cossi, J. M. Millam, M. Klene, C. Adamo, R. Cammi, J. W. Ochterski, R. L. Martin, K. Morokuma, O. Farkas, J. B. Foresman, D. J. Fox, *Gaussian 09 Rev. E.01*, Gaussian Inc, Wallingford, CT, **2009**.
- [28] S. Gozem, A. I. Krylov, *WIREs Comput. Mol. Sci.* **2022**, *12*, e1546.

Manuscript received: May 5, 2022

Accepted manuscript online: May 27, 2022

Version of record online: June 24, 2022